Effects of the interface roughness in metal-adhesive-metal structure on the propagation of shear horizontal waves

Mounsif Ech Cherif El Kettani, Damien Leduc, Catherine Potel, Michel Bruneau, Ludovic Foze, Mihai Predoi

Effects of the interface roughness in metal-adhesive-metal structure on the propagation of shear horizontal waves

Mounsif Ech Cherif El Kettani and Damien Leduc[a)]
Laboratoire Ondes et Milieux Complexes, Unité Mixte de Recherche CNRS 6294, University of Normandy, Le Havre, France

Catherine Potel, Michel Bruneau, and Ludovic Foze
Laboratoire d'Acoustique de l'Université du Maine, Unité Mixte de Recherche CNRS 6613, University of Maine, Le Mans, France

Mihai Predoi
Department of Mechanics, University Politehnica of Bucharest, Splaiul Independentei, 313, Sect. 6, 060042 Bucharest, Romania

(Received 21 December 2016; revised 2 May 2017; accepted 30 May 2017; published online 20 June 2017)

The influence of the interface roughness in a three-layer metal-adhesive-metal structure on the propagation of shear horizontal waves and more particularly on the transmission coefficient versus the frequency is studied in the particular case of a periodic grating of triangular grooves. For given phonon frequencies, the interaction of an incident shear horizontal mode with the periodical grating gives rise to a retro-converted mode. A numerical finite element simulation permits us to predict the existence of the phonon mode in the three-layer structure and to obtain the evolution of the transmission coefficient around the phonon frequency. An experimental study, based on a generation of waves by a piezocomposite contact transducer and a reception by a laser vibrometer, then confirms these predictions. Finally, a parametric numerical study is performed: the influence of the depth of the roughness and of the number of spatial periods of the grooves on the transmission coefficient is studied. © *2017 Acoustical Society of America*. [http://dx.doi.org/10.1121/1.4985441]

[MD] Pages: 4591–4599

I. INTRODUCTION

Ultrasonic waves are widely used in non-destructive testing and evaluation (NDT/NDE), including the control of adhesive bonding between surfaces which are usually roughened in order to enhance the quality of the adhesion (e.g., see Refs. 1–3). Numerous articles[4–20] deal with the propagation of ultrasonic guided waves in rough plates, and more particularly on the topic of ultrasonic non-destructive evaluation of adhesive bonds, using either longitudinal or shear bulk waves,[21–25] Lamb or Shear-Horizontal (SH) guided waves.[26–29] The present paper follows the article of Potel *et al.*,[30] which is an analytical contribution to the study of the scattering effects of roughness on the propagation of SH-waves inside two plates stuck by a layer of glue. This contribution takes into account the shape and the depth of the roughness, among other parameters. The present paper provides a numerical simulation (using finite element method) and an experimental contribution to the study of the interaction of an incident SH wave with a periodic grating (of triangular grooves) in a three-layer structure (metal-adhesive-metal), more specifically when the phase matching (versus frequency) of the incident SH wave with the roughness occurs, giving in particular the evolution of the transmission coefficient in the vicinity of the phonon frequency. To the authors knowledge, no work has been yet devoted to these two last points, because the phonon relation influence being studied only in the case of a single plate until now.[11,13,18–20]

II. MATERIALS

Subsequently, the investigated bonded structure is a three-layer Aluminum-Araldite-Aluminum structure which is 400 mm length following the x axis (see Fig. 1) and 10.5 mm thick. The bonded surfaces of the two Aluminum plates are separated into three zones: two smooth areas upstream and downstream the roughness, and a rough area, as shown on Fig. 1. The roughness profile at the surface of the two plates is a periodic distribution of ten contiguous triangular grooves with a spatial period $\Lambda = 3.7$ mm. The depth of the grooves is $H = 0.1$ mm. The length of the zones explored before and after the roughness is 40 mm, the length of the rough area being always 37 mm. The geometrical and physical parameters of the plates and of the adhesive are given in Table I.

III. DISPERSION CURVES

A one-dimensional Semi Analytical Finite Element (SAFE) model solved here with Comsol software[31–34] allows to provide numerically the eigenvalue problem, associated to the wave equation and the boundary conditions. It gives the dispersion curves (dots on Fig. 2) of the studied three-layer structure without roughness (represented by its cross-section), assuming perfect adhesion hypothesis and structure in vacuum. On the other hand, the analytical dispersion curves

[a)]Electronic mail: damien.leduc@univ-lehavre.fr

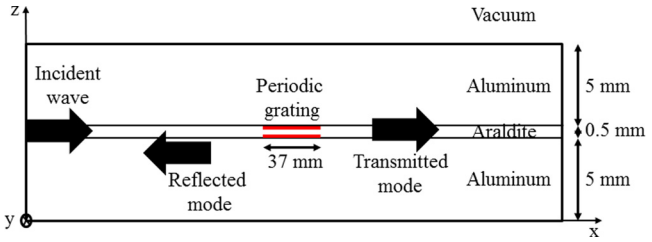

FIG. 1. (Color online) Geometry of the studied sample.

are obtained by minimizing the determinant of the system resulting from the boundary conditions in the perfect adhesion hypothesis (full line on Fig. 2). The numerical study is done frequency by frequency. For each frequency, the eigenvalues are calculated. So, we obtain for the studied frequencies the values of the wave numbers of the SH modes (black points on Fig. 2). The three-layer modes are labeled SH_0, SH_1, SH_2,… according to ascending cut-off frequencies. There is a very good agreement between the two solving methods.

IV. EFFECTS OF THE PHASE MATCHING BETWEEN THE INCIDENT AND THE CONVERTED MODES

Roughness, characterized here by its spectrum power density,[20] involves coupling phenomena between guided modes.[17–19] Reflected guided mode which propagates in the same direction as incident mode (co-directional coupling) and reflected mode which propagates in the opposite direction (contra-directional coupling) are considered.[35,36] These energy transfer mechanisms between modes are subject to a phase matching condition linking wavelengths of one or two guided modes with the spatial periodicity of the roughness.[35,36] This condition, called phonon relation,[11,13,18–20] is expressed as

$$k_{x_I} \pm k_{x_R} - \frac{2n\pi}{\Lambda} = 0, \tag{1}$$

where k_{x_I} and k_{x_R} are the wave numbers of the incident and reflected modes, respectively, and where n is a nonzero integer which is associated to a harmonic of the spatial periodicity Λ of the roughness, and where the sign of the wave number k_{x_R} indicates the propagation direction of the mode (the sign + indicates a contra-directional coupling and the sign - a co-directional coupling). This condition is verified for a given frequency, called phonon frequency, and provides maximum coupling between the incident mode and the converted mode.

A. Phonon curves

The objective is here to generate SH converted mode at a phonon frequency in the three-layer structure Aluminum-Araldite-Aluminum, with rough interfaces composed of ten

TABLE I. Geometrical and physical parameters of the Aluminum plates and of the glue.

	Aluminum plates	Glue (Araldite)
Lamé second constant μ (GPa)	26.003	2.133
Density ρ (kg m^{-3})	2705.8	1160
Shear wave velocity c_T (m s^{-1})	3100	1356
Thickness L (mm)	5	0.5

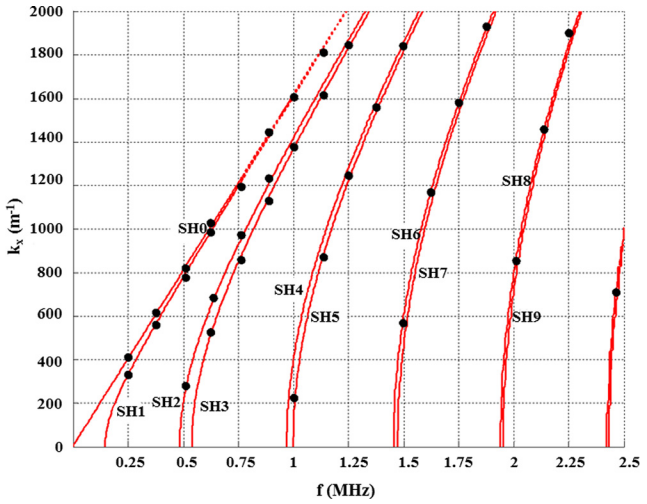

FIG. 2. (Color online) Dispersion curves of the three-layer structure (Fig. 1 and Table I): analytical method (red line), SAFE method (dots).

triangular grooves (see Sec. II). The intersections between the dispersion curves and the phonon curves defined by the phonon relation

$$g(f) = 2\pi/\Lambda - k_{x_R}, \tag{2}$$

expressed as a function of frequency f, represent a phase matching, i.e., maximum coupling between two modes (see Fig. 3, where the red lines correspond to the dispersion curves of the incident mode and the blue lines correspond to the phonon curves of the converted modes). For example, the SH_0 incident mode (red line) is in phonon relation with the retro-converted (or contra-directional) SH_2 mode (blue line) at a phonon frequency of 480 kHz. Similarly, the incident SH_2 mode is in phonon relation with the retro-converted SH_4 mode at a phonon frequency of 670 kHz.

B. Numerical study of the SH_0 incident mode in phonon relation with the retro-converted SH_2 mode

The numerical FEM study conducted here is a predictive model for the experimental study. The model provides the

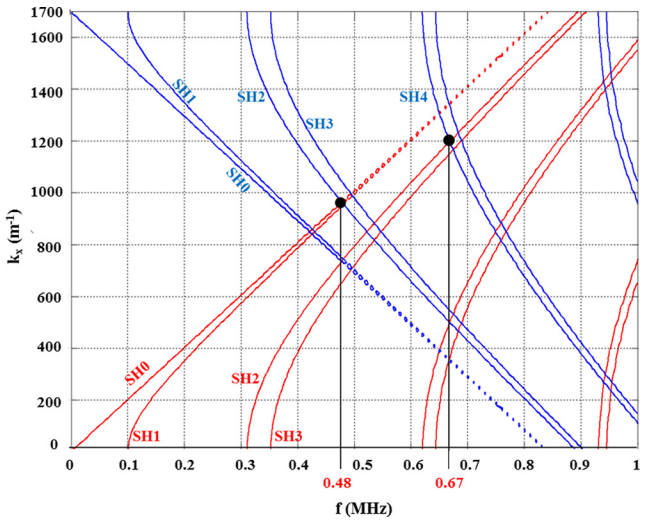

FIG. 3. (Color online) Dispersion curves of the incident mode and phonon curves of the converted modes.

displacement of a SH wave, polarized following the y axis in the xz-plane of the section of the considered three-layer structure (Fig. 1). The most intuitive and straightforwardly applicable method for an experimental validation is the simulation of the wave propagation as a function of time. The main advantage is that the same signal processing tools can be applied for obtaining the numerical and experimental results. On the other hand, the disadvantage is the relatively large computer memory requirements and the duration of the computation. A correct meshing with a sufficient number of cells per wavelength should be taken to respect the Shannon condition. In our case, the mesh consists in taking 10 to 20 elements per wavelength, which is a good compromise between a good spatial sampling and a correct resolution time. To generate a given mode, the U_y displacement field obtained in the 1D model (see Sec. III) is applied on the left section of the two-dimensional (2D) model. The displacement of the mode is multiplied by a harmonic signal of n periods and applied to the left section of the three-layer structure. The time function describing the applied signal is given by

$$F(t) = \sin(\omega t) \quad \text{for } 0 \le t \le nT, \tag{3}$$

where $\omega = 2\pi f$ is the excitation angular frequency and nT ($T = 1/f$ is the signal period) represents the duration of the excitation. The displacement field of the SH_0 mode at a given frequency, obtained from the SAFE model, is applied on the $x = 0$ section of the whole three-layer structure, in order to ensure a pure mode excitation. The input signal is a burst of three periods [n = 3 in Eq. (3), central frequency equal to 480 kHz], which allows a wide frequency band around the central frequency. The model is calculated in transient regime with propagation duration of 45 μs, which is enough for the incident mode to reach the end of the structure. The time varying shear displacements on the upper free surface of the structure are extracted from the FEM solution, at equally spaced positions with a 0.1 mm step and stored in a time-position-amplitude matrix. A spatio-temporal representation of the shear displacement is shown in Fig. 4. The studied length along the Ox axis corresponds to the 117 mm distance that will be explored experimentally.

Spatial and temporal FFT are performed on the data collected before the roughness, for a propagation distance of 27 mm. Signal processing is not done for the signals near the rough area in order to avoid transients associated with the change of the propagation medium properties. The result of the 2D FFT is presented on Fig. 5 for the incident mode, and on Fig. 6 for the retro-converted mode. The temporal FFT is performed on 32 768 points and the spatial FFT is performed on 16 384 points. The aim is to respect the Nyquist-Shannon sampling theorem that is largely the case here. We use the zero-padding technique to improve the localization of the maxima of the spectrum. In our case, the numbers of points allow to obtained a resolution of $\Delta f = 878.9$ Hz and $\Delta k = 3.835\ \text{m}^{-1}$, largely sufficient to determine with a good accuracy the frequency and the wave number that are on the order of 400–500 kHz and of 800–1000 m^{-1}, respectively.

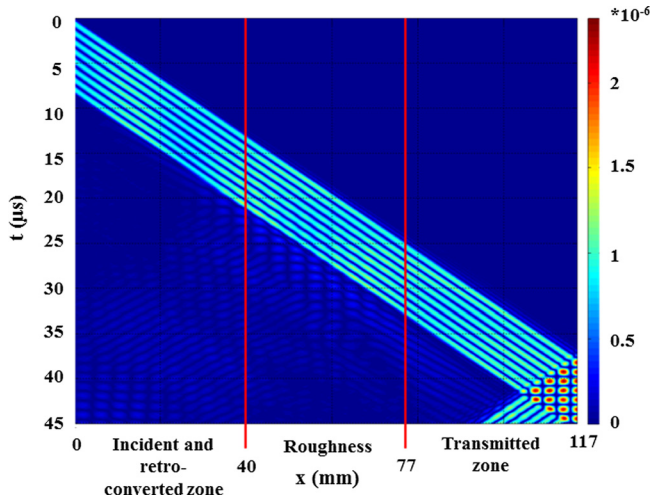

FIG. 4. (Color online) Spatio-temporal representation of the surface displacements (numerical simulation). The color amplitude is in arbitrary unit.

Please note that the calculation of the 2D FFT with these numbers of points last less than 1 min with a standard computer (processor Intel I5, 16 Go RAM). The same procedure is performed on the data after the roughness. On Fig. 5 the red spot permits to identify the incident SH_0 mode centered around the frequency $f = 480$ kHz. The retro-converted SH_2 mode is identified at the same frequency ($f = 480$ kHz, phonon frequency) in Fig. 6 for negative values of the wave number. The results of the numerical simulations are in good agreement with the theoretical predictions [Eq. (1)]. Moreover, the amplitude associated to the retro-converted mode (Fig. 6) is one tenth that of the incident mode (Fig. 5), which could make its experimental detection difficult. Note that (Table II) SH_0 and SH_2 modes satisfy the phonon relation [Eq. (1)]. Figure 7 shows the results of the 2D FFT performed on the transmitted signals (collected downstream the roughness). As expected, the transmitted SH_0 mode is observed centered around the frequency $f = 480$ kHz.

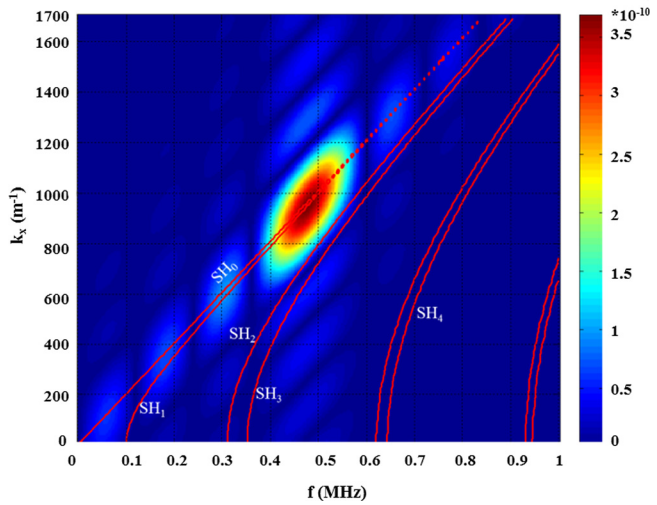

FIG. 5. (Color online) 2D FFT of the incident signal (upstream the roughness) – SH_0 incident mode generated – the dispersion curves of the three-layer in red (numerical simulation). The color amplitude is in arbitrary unit.

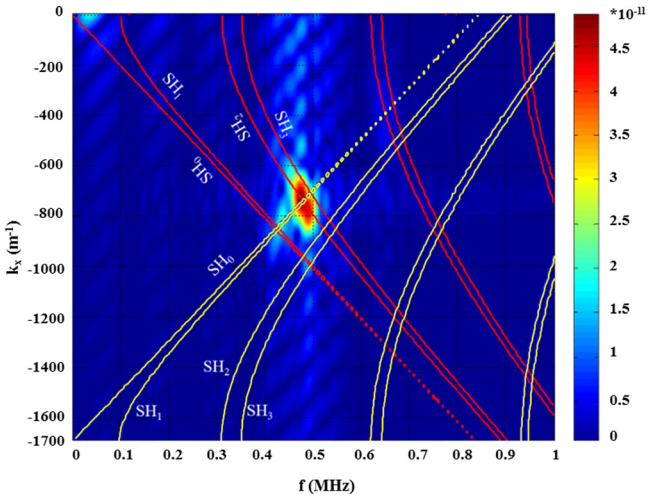

FIG. 6. (Color online) 2D FFT of the reflected signals by the roughness (upstream the roughness): SH_2 reflected mode. Dispersion curves of the three-layer structure and phonon curves (numerical simulation). The color amplitude is in arbitrary unit.

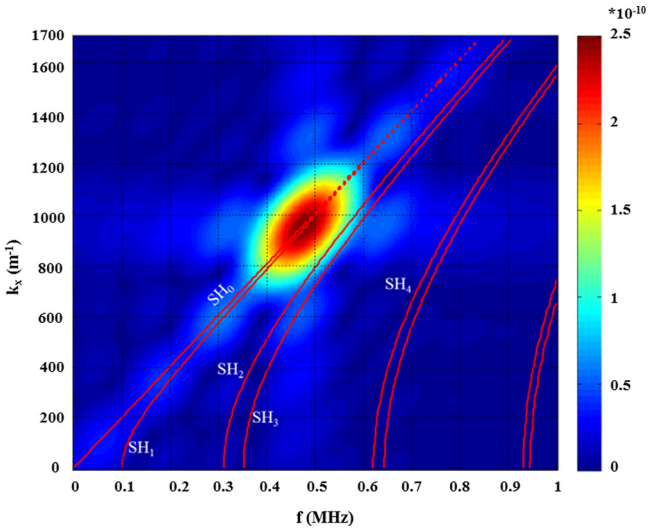

FIG. 7. (Color online) 2D FFT of the transmitted signals (downstream the roughness): SH_0 transmitted mode. Dispersion curves of the three-layer structure in red and phonon curves in blue (numerical simulation). The color amplitude is in arbitrary unit.

C. Evolution of the transmission coefficient versus frequency

In this section, we are interested in the evolution of the amplitude transmission coefficient as a function of the frequency, in the aim to study its particular behavior around the phonon frequency. This transmission coefficient is defined as the ratio of the maximum amplitude of the 2D FFT of the transmitted mode (Fig. 7) to the maximum amplitude of the 2D FFT of the incident mode (Fig. 5), at a given frequency. The maximum amplitudes of the 2D FFT are obtained by making cuts at different frequencies centered on the phonon frequency (Figs. 5 and 7). The frequency step between two cuts is 5 kHz, greater than the frequential resolution of the FFT ($\Delta f = 879$ Hz). The blue line in Fig. 8 shows the evolution of the amplitude transmission coefficient as function of the frequency, around the phonon frequency $f = 480$ kHz (numerical simulation). Note that the amplitude transmission coefficient is minimum at the phonon frequency. This can be explained by the fact that, at the phonon frequency, the reflections due to the roughness are in phase matching and thus a retro-converted SH mode is generated. This reflected mode carries more energy than when these reflections are not in phase matching, which happens out of the phonon frequency. This result has to be validated in the following experimental study (Sec. IV D).

D. Experimental results

The experimental setup is presented on Fig. 9. The geometrical and physical parameters (Table I) of the sample are the same as in the FEM study. A shear wave transducer (manufacturer: Valpey Fisher) creates the incident field (central frequency equal to 500 kHz, frequency bandwidth at −6 dB equal to 400 kHz). The transducer is placed on a Plexiglas wedge inclined (25°) with regard to the plate surface. The structure is rotated of an angle of 45° versus the xy plane around the z axis (the laser beam is perpendicular to the xy plane) and a reflector film is placed on the surface along the acoustic beam direction. This configuration allows measurements of the amplitude of the shear displacement,[37] with a weighting factor equal to $\sqrt{2}/2$. The time varying signals due to the propagating SH wave are measured by a laser velocimeter (manufacturer: Polytec), with a sensitivity of 20 V/(m s^{-1}). The laser is translated in the propagation direction, by steps of 0.1 mm, over 150 mm distance. For each position, the signal acquisition is done over 200 μs duration, corresponding to 20 000 time samples. The size of the time-position matrix is thus 20 000 rows and 1500 columns. The lengths of the areas explored upstream and downstream the roughness are 50 mm and 63 mm, respectively, the roughness length being 37 mm. The experiment is carried out with a quasi-harmonic excitation signal of three cycles with a central frequency of $f = 480$ kHz, as in the numerical study. The transducer is excited with only few cycles in order to have a broad spectrum around the central frequency of the burst [see Fig. 10(a)]. The amplitude of the transverse displacement at the different positions is shown as a function of time in Fig. 10(b). The method used to identify and to separate the SH modes generated in the three-layer structure is

TABLE II. Phonon relation between the SH_0 incident mode and the SH_2 retro-converted mode at $f = 480$ kHz.

	Incident mode $k_x SH_0$ (m^{-1})	Retro-converted mode $k_x SH_2$ (m^{-1})	Spatial wavelength of the roughness $2\pi/\Lambda$ (m^{-1})	Relative error between Σk_x and $2\pi/\Lambda$
Simulation	940	750	1700	0.5%
Experiment	945	740	1700	0.9%

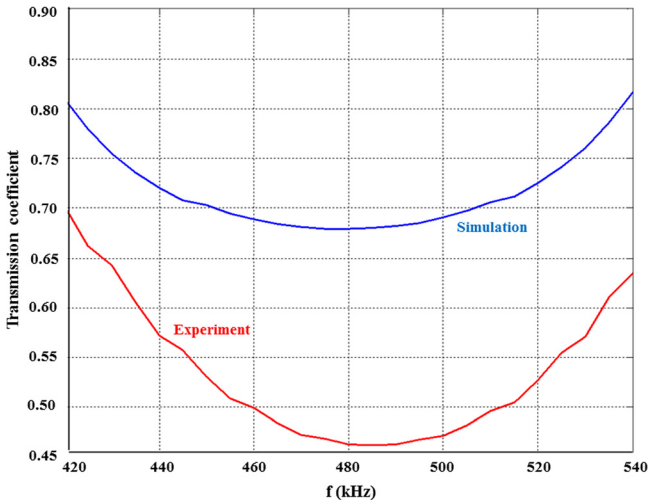

FIG. 8. (Color online) Evolution of the amplitude transmission coefficient versus frequency: numerical simulation and experimental results.

the same as in the numerical simulations. The 2D FFT of the incident signal upstream the roughness is shown in Fig. 10(c): the SH_0 mode is identified, centered around $f = 480$ kHz. The mode propagated at $x = 0$ between 70 and 80 μs [Fig. 10(b)] is SH0 too (the 2D FFT of this signal shows a spot in the same frequency-wave number range) but probably generated by a reflection in the Plexiglas wedge. Please note that the 2D FFT [Fig. 10(c)] is performed only on the signal between 30 and 70 μs in the incident area, without taking into account the reflection in the Plexiglas wedge. For the negative values of k_x the 2D FFT signal in the zone downstream the roughness allows identifying the SH_2 retro-converted mode at the frequency 480 kHz [Fig. 11(a)], as predicted by the numerical simulations. The experimental observation of this retro-converted mode, even if it was predicted, is not trivial for two reasons: first, the amplitude associated to this mode is very weak as shown in the numerical

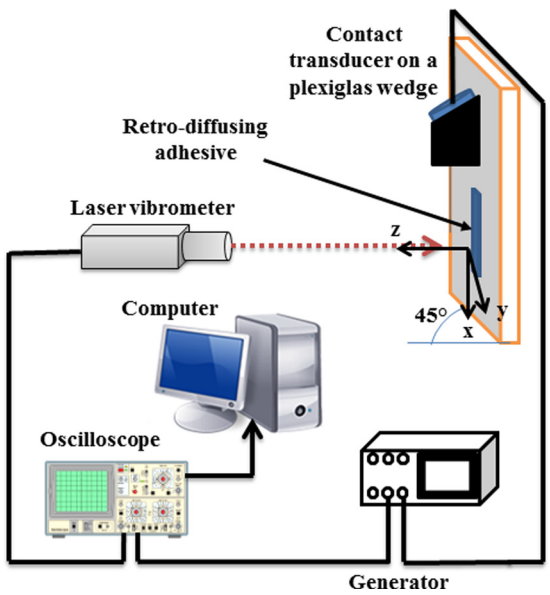

FIG. 9. (Color online) Experimental setup.

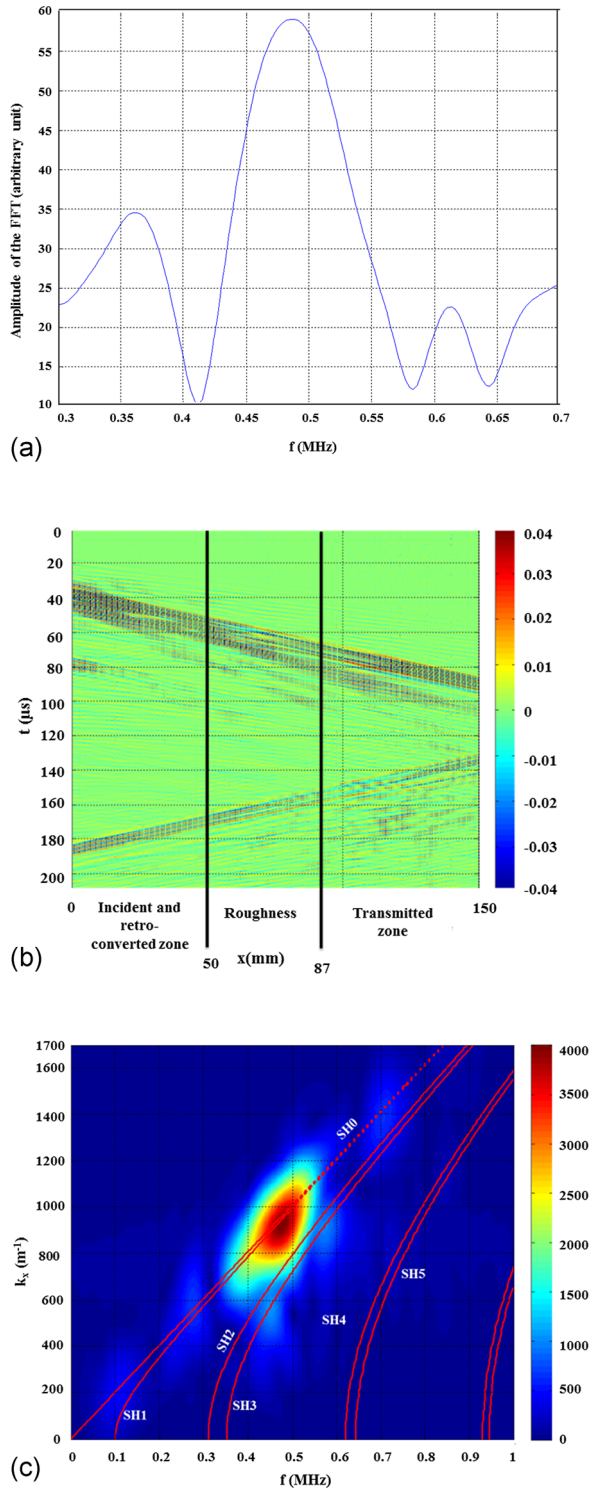

FIG. 10. (Color online) (a) Amplitude of the FFT of the excitation signal (experimental result). The amplitude is in arbitrary unit. (b) Time-space representation of the displacements at the surface of the three-layer (experimental result). The color amplitude is in arbitrary unit. (c) 2D FFT of the incident signal (before roughness) – SH_0 incident mode generated – Dispersion curves of the three-layer in red (experimental result). The color amplitude is in arbitrary unit.

study, and second, only a proportion of the amplitude of the propagating SH wave is measured by the laser. Table II shows that the SH_0 and SH_2 modes satisfy the phonon relation. The 2D FFT of the transmitted signal is shown in Fig. 11(b).

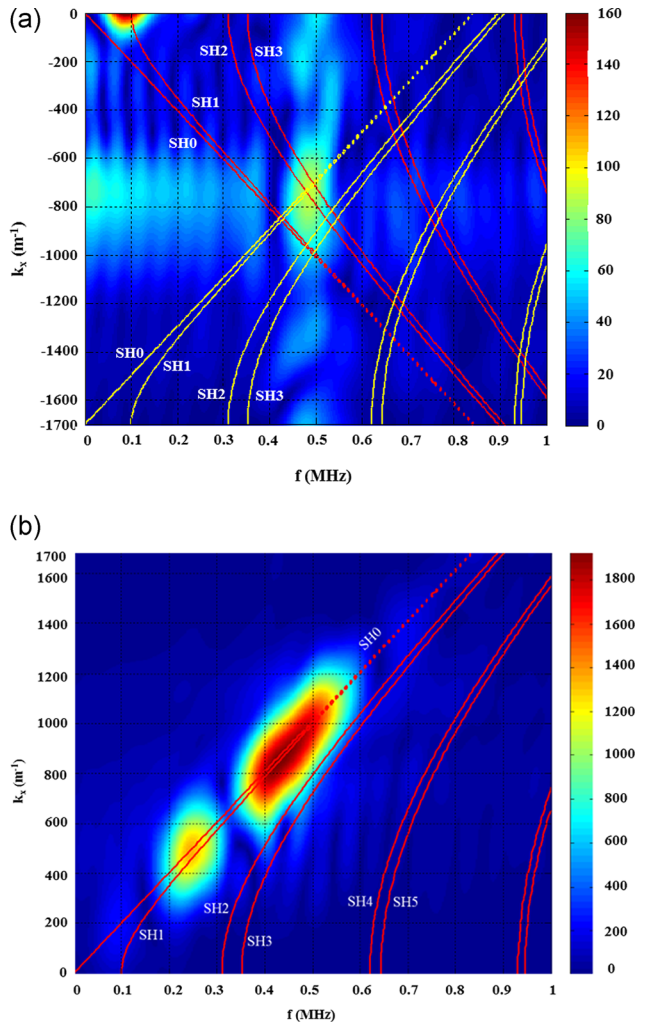

FIG. 11. (Color online) (a) 2D FFT of the reflected signal by the roughness (before the roughness): SH_2 reflected mode. Dispersion curves of the three-layer structure and phonon curves (experimental results). The color amplitude is in arbitrary unit. (b) 2D FFT of the transmitted signal (after the roughness): SH_0 transmitted mode. Dispersion curves of the three-layer structure (experimental results). The color amplitude is in arbitrary unit.

An experimental amplitude transmission coefficient is calculated, in the same way as in the numerical study. The result is reported on Fig. 8 and is compared to the numerical amplitude transmission coefficient, as a function of the frequency: both coefficients exhibit the same behavior versus frequency, with a minimum at the phonon frequency. However, the experimental values of the transmission coefficient are lower than those obtained in the numerical simulations. This can be explained by the geometrical aperture of the beam during the wave propagation which is not taken into account in the numerical study. In addition, the displacement obtained from experiments is not exactly that obtained on the surface from the numerical in simulation, but is rather a part of this displacement due to the angle 45° mentioned above. Nevertheless, the physical phenomenon of interest being the minimum reached by the transmission coefficient at the phonon frequency, the numerical FEM model can thus be considered as validated. In the next section, Sec. IV E, the SH_0 mode which is in phonon relation with the retro-converted SH_0 mode is studied in order to confirm these results.

E. Study of the SH_0 mode in phonon relation with the retro-converted SH_0 mode

The three-layer and the simulation parameters are the same as previously. The SH_0 mode is generated at

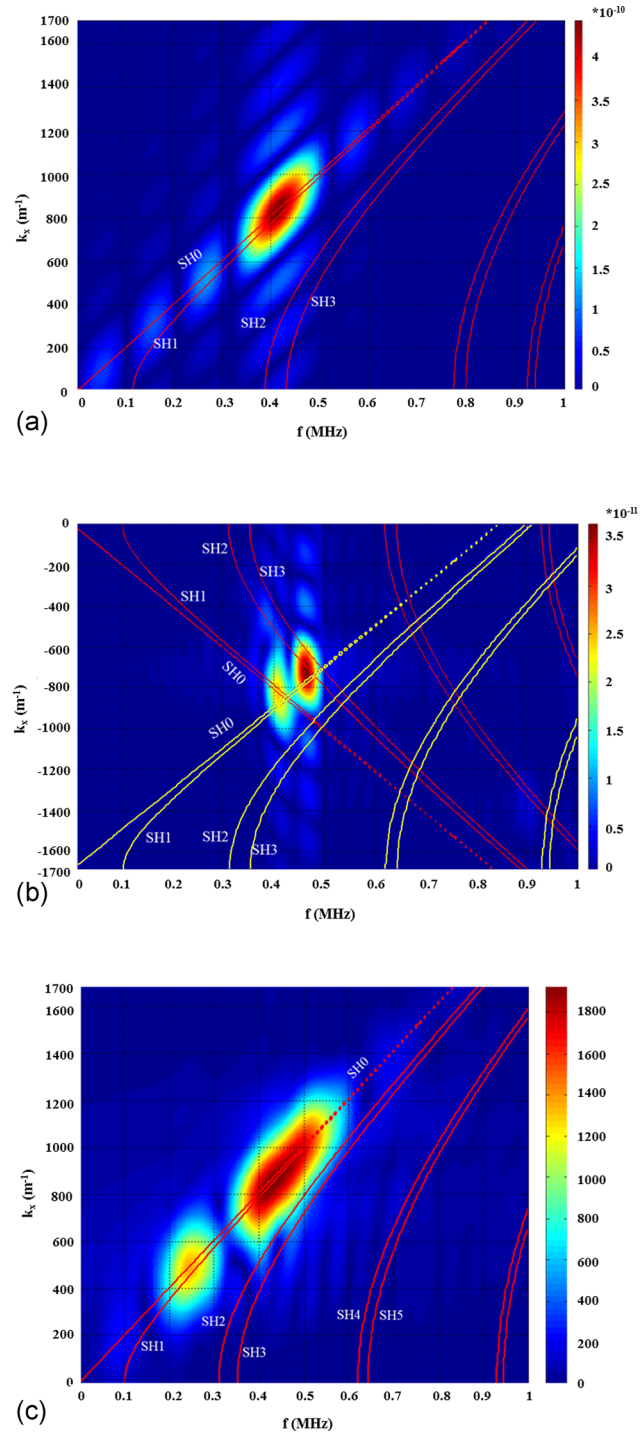

FIG. 12. (Color online) (a) 2D FFT of the incident signal (before the roughness): SH_0 incident mode. Dispersion curves of the three-layer (numerical simulation). The color amplitude is in arbitrary unit. (b) 2D FFT of the reflected signal by the roughness (before the roughness): SH_0 reflected mode. Dispersion curves of the three-layer structure and phonon curves (numerical simulation). The color amplitude is in arbitrary unit. (c) 2D FFT of the transmitted signal (after the roughness): SH_0 transmitted mode. Dispersion curves of the three-layer (numerical simulation). The color amplitude is in arbitrary unit.

TABLE III. Phonon relation between SH_0 incident mode and SH_0 retro-converted mode at $f = 420$ kHz.

Incident mode k_xSH_0 (m^{-1})	Retro-converted mode k_xSH_0 (m^{-1})	Spatial wavelength of the roughness $2\pi/\Lambda$ (m^{-1})	Relative error between Σk_x and $2\pi/\Lambda$
940	730	1700	1,7%

$f = 420$ kHz for $k_x = 840\ m^{-1}$. The same signal processing allows identifying the generated and retro-converted modes [Figs. 12(a) and 12(b)]. The 2D FFT of the transmitted signal is shown in Fig. 12(c). In Fig. 12(b), two phonons are observed: the first one is the phonon expected to be around $f = 420$ kHz (SH_0 incident mode in phonon relation with SH_0 retro-converted mode) and another phonon around $f = 480$ kHz corresponding to this observed in the previous study (SH_0 in phonon relation with SH_2). This can be explained by the fact that the frequency $f = 480$ kHz is included in the spectrum of the incoming signal [see Fig. 12(a), the spectrum ranges from 350 kHz to 500 kHz]. Table III shows that the SH_0 mode is in phonon relation with himself. The amplitude transmission coefficient is calculated as previously and is plotted versus frequency in Fig. 13. As expected, the transmission coefficient is minimum at the phonon frequency ($f = 420$ kHz). This second numerical result confirms this physical phenomenon again. In Sec. IV F, we study the influence of the geometrical parameters of the roughness on the transmitted signal.

F. Influence of the geometrical parameters of the roughness on the transmitted signal

1. Influence of the roughness depth

The geometrical and physical parameters of considered structure are those given in Table I. Three roughness depths, selected to remain in the hypothesis of small perturbations i.e., there are small compared to the thickness of the plates, are in this study: 0.1, 0.05, and 0.02 mm. The roughness length remains fixed ($L = 37$ mm). The corresponding numerical results for the amplitude transmission coefficient as a function of the frequency are shown in Fig. 14. Note that the transmission coefficient increases and has a less marked minimum when the depth of the surface roughness decreases. Indeed for a roughness depth equal to zero (no roughness), the transmission coefficient is equal to 1, because attenuation is not taken into account in the modeling.

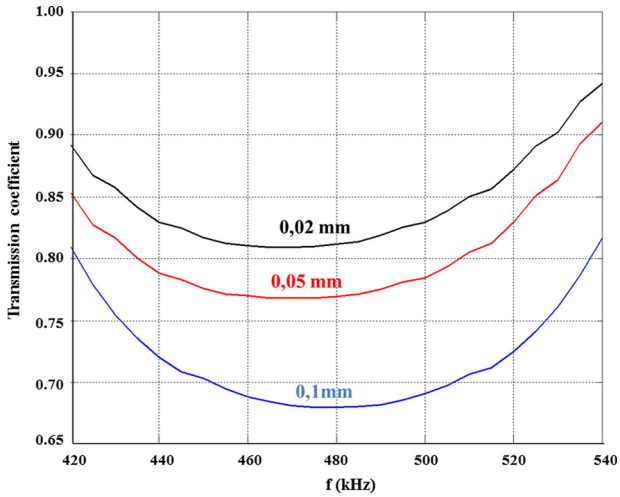

FIG. 14. (Color online) Influence of the roughness depth on the amplitude transmission coefficient (numerical simulation).

2. Influence of the roughness length on the transmitted signal

In this study, the depth of roughness remains fixed ($H = 0.1$ mm), the roughness lengths being 37 mm (10 grooves, i.e., 10Λ), 22.2 mm (6 grooves, i.e., 6Λ), 11.1 mm (3 grooves, i.e., 3Λ), and 3.7 mm (one groove, i.e., Λ). The retro-converted mode is always observed around $f = 480$ kHz (even for two grooves), except when there is only one groove (no more periodicity). The corresponding transmission coefficients increase as the roughness length decreases (Fig. 15) and reach the value 1 when the roughness is cancelled.

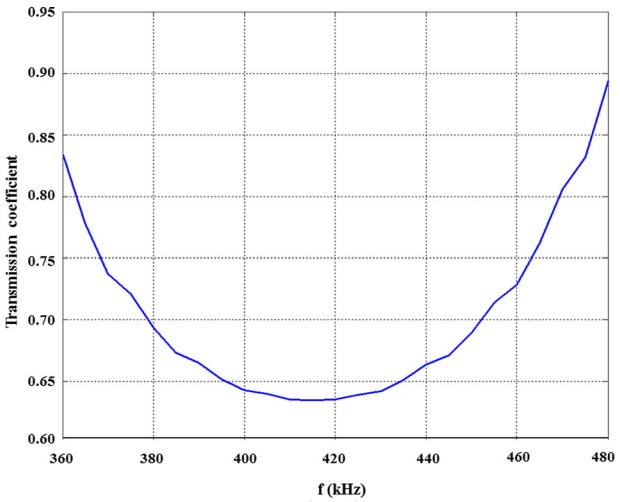

FIG. 13. (Color online) Evolution of the amplitude transmission coefficient versus frequency (numerical simulation).

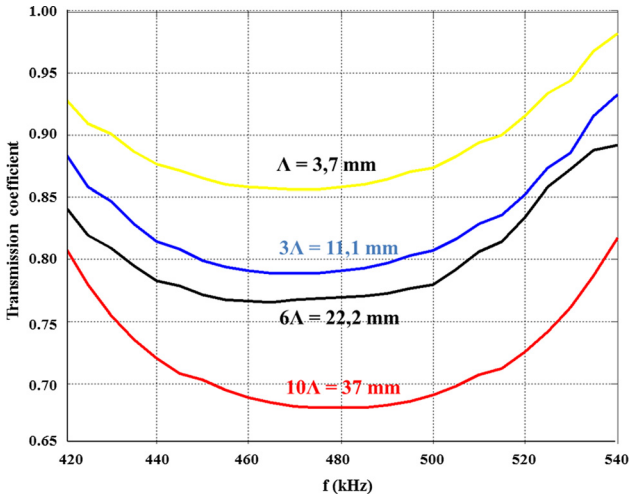

FIG. 15. (Color online) Influence of the roughness length on the amplitude transmission coefficient (numerical simulation).

V. CONCLUSIONS

The propagation of SH modes in a three-layer structure (Aluminum-Araldite-Aluminum) with rough interfaces, the profile of which is a periodic distribution of triangular grooves has been considered. The dispersion curves for the SH modes in the structure with smooth interfaces are first determined using the SAFE method. A predictive numerical model (FEM simulation) for the structure with rough interfaces is then developed in the time domain. Experiments are finally carried out, using a set-up which allows measuring the surface displacement parallel to the surfaces of the plate. Analysis of the time-space representations of the incident and transmitted signals leads to the detection of a phonon mode and allows studying the evolution of the amplitude transmission coefficients versus frequency. The numerical and experimental curves of the transmission coefficients exhibit a minimum at the phonon frequency. Finally, two parametric analysis show the influence of the depth and the length of the roughness on the transmitted signal: the first analysis shows the decrease in the amplitude of the retro-converted mode with decreasing roughness depth and the second one shows the presence or absence of a retro-converted mode when the grating is periodic or not respectively.

To the authors knowledge, this is the first time that the existence of a phonon mode for a three-layer structure and with SH wave is highlighted experimentally. The difficulty lays in the fact that the transverse wave transducers generate SH waves with lower energy than the longitudinal ones. Another difficulty is that only a small part of the 45° component of displacement is measured as the backscattering adhesive film diffracts the signal in all directions.

ACKNOWLEDGMENTS

This work was supported by the ANR grant ISABEAU (project ANR 12-BS-09-0022-01). The authors want to thank Camille Gauthier for machining the samples.

[1]C. C. H. Guyott, P. Cawley, and R. D. Adams, "The non-destructive testing of adhesively bonded structure: A review," J. Adhes. **20**,129–159 (1986).
[2]P. B. Nagy and L. Adler, "Nondestructive evaluation of adhesive joints by guided waves," J. Appl. Phys. **66**(10), 4658–4663 (1989).
[3]M. Lowe and P. Cawley, "The applicability of plate wave techniques for the inspection of adhesive and diffusion bonded joints," J. Nondestr. Eval. **13**, 185–200 (1994).
[4]O. I. Lobkis and D. E. Chimenti, "Elastic guided waves in plates with surface roughness I Model calculation," J. Acoust. Soc. Am. **102**, 143–149 (1997).
[5]O. I. Lobkis and D. E. Chimenti, "Elastic guided waves in plates with surface roughness II experiments," J. Acoust. Soc. Am. **102**, 150–159 (1997).
[6]D. E. Chimenti and O. I. Lobkis, "The effect of rough surfaces on guided waves in plates," Ultrasonics **36**, 155–162 (1998).
[7]S. Dai and H. Zhang, "Propagation of elastic waves in a plate with rough surfaces," Chin. J. Acoust. **22**(3), 194–202 (2003).
[8]S. Banerjee and T. Kundu, "Elastic wave propagation in sinusoidally corrugated waveguides," J. Acoust. Soc. Am. **119**, 2006–2017 (2006).
[9]S. Banerjee and T. Kundu, "Symmetric and anti-symmetric Rayleigh-Lamb modes in sinusoidally corrugated waveguides: An analytical approach," Int. J. Solids Struct. **43**, 6551–6567 (2006).
[10]W. Lauriks, L. Kelders, and J. F. Allard, "Surface waves above gratings having a triangular profile," Ultrasonics **36**, 865–871 (1998).
[11]B. Morvan, A.-C. Hladky-Hennion, D. Leduc, and J.-L. Izbicki, "Ultrasonic guided waves on a periodical grating: Coupled modes in the first Brillouin zone," J. Appl. Phys. **101**(1), 114906 (2007).
[12]M. Bavencoffe, A. Hladky-Hennion, B. Morvan, and J. Izbicki, "Attenuation of Lamb waves in the vicinity of a forbidden band in a phononic crystal," IEEE Trans. Ultrason. Ferroelectr. Freq. Control **56**(9), 1960–1967 (2009).
[13]D. Leduc, A.-C. Hladky-Hennion, B. Morvan, J.-L. Izbicki, and P. Pareige, "Propagation of Lamb waves in a plate with a periodic grating: Interpretation by phonon," J. Acoust. Soc. Am. **118**(4), 2234–2239 (2005).
[14]C. Potel and M. Bruneau, "Modes coupling due to nonhomogeneously shaped walls in duct acoustics," J. Sound Vib. **313**, 738–759 (2008).
[15]T. Valier-Brasier, C. Potel, and M. Bruneau, "On the modeling of modes coupling in dissipative fluid-filled waveguide with corrugated surfaces," J. Appl. Phys. **106**(3), 034913 (2009).
[16]D. Leduc, B. Morvan, A.-C. Hladky-Hennion, P. Pareige, and J.-L. Izbicki, "Lamb wave propagation in a plate with a grooved surface with several spatial periodicities," Ultrasonics **44**, 1359–1363 (2006).
[17]C. Potel, D. Leduc, B. Morvan, C. Depollier, A.-C. Hladky-Hennion, J.-L. Izbicki, P. Pareige, and M. Bruneau, "Lamb wave attenuation in a rough plate. I. Analytical and experimental results in an anisotropic plate," J. Appl. Phys. **104**(7), 074908 (2008).
[18]C. Potel, D. Leduc, B. Morvan, C. Depollier, A.-C. Hladky-Hennion, J.-L. Izbicki, P. Pareige, and M. Bruneau, "Lamb wave attenuation in a rough plate. II. Analytical and numerical results in a fluid plate," J. Appl. Phys. **104**(7), 074909 (2008).
[19]T. Valier-Brasier, C. Potel, and M. Bruneau, "Modes coupling of shear acoustic waves polarized along a one-dimensional corrugation on the surfaces of an isotropic solid plate," Appl. Phys. Lett. **93**(16), 164101 (2008).
[20]D. Leduc, B. Morvan, A.-C. Hladky-Hennion, and J.-L. Izbicki, "Interaction of Lamb waves with a grating composed of two spatial periodicities: Study in dual space," NDT&E Int. **42**(6), 513–517 (2009).
[21]S. I. Rokhlin and D. Marom, "Study of adhesive bonds using low-frequency obliquely incident ultrasonic waves," J. Acoust. Soc. Am. **80**, 585–590 (1986).
[22]A. Pilarski and J. L. Rose, "Ultrasonic oblique incidence for improved sensitivity in interface weakness determination," NDT Int. **21-4**, 241–246 (1988).
[23]F. J. Margetan, R. B. Thompson, J. H. Rose, and T. A. Gray, "The interaction of ultrasound with imperfect interfaces: Experimental studies of model structures," J. Nondestruct. Eval. **11**, 109–125 (1992).
[24]B. W. Drinkwater and P. Cawley, "Measurement of the frequency dependence of the ultrasonic reflection coefficient from thin interface layers and partially contacting interfaces," Ultrasonics **35**, 479–488 (1997).
[25]S. Dixon, D. Jaques, S. B. Palmer, and G. Rowlands, "The measurement of shear and compression waves in curing epoxy adhesives using ultrasonic reflection and transmission techniques simultaneously," Meas. Sci. Technol. **15**, 939–947 (2004).
[26]K. Heller, L. J. Jacobs, and J. Qu, "Characterization of adhesive bond properties using Lamb waves," NDT&E Int. **33**, 555–563 (2000).
[27]M. J. S. Lowe, R. E. Challis, and C. W. Chan, "The transmission of Lamb waves across adhesively bonded lap joints," J. Acoust. Soc. Am. **107**, 1333–1345 (2000).
[28]R. Seifried, L. J. Jacobs, and J. Qu, "Propagation of guided waves in adhesive bonded components," NDT&E Int. **35**, 317–328 (2002).
[29]F. Lanza di Scalea and P. Rizzo, "Propagation of ultrasonic guided waves in lap-shear adhesive joints: Case of incident A0 Lamb wave," J. Acoust. Soc. Am. **115**, 146–157 (2004).
[30]C. Potel, M. Bruneau, L. Foze Ndjomo, D. Leduc, M. Ech Cherif El Kettani, and J.-L. Izbicki, "Shear horizontal acoustic waves propagating along two isotropic solid plates bonded with a non-dissipative adhesive layer: Effects of the rough interfaces," J. Appl. Phys. **118**(22) 224904 (2015).
[31]A. Marzani, E. Viola, I. Bartoli, F. L. D. Scaela, and P. Rizzo, "A semi-analytical finite element formulation for modeling stress wave propagation in axisymmetric damped waveguides," J. Sound Vib. **318**, 488–505 (2008).
[32]M. Koshiba, K. Hasegawa, and M. Suzuki, "Finite-Element solution of horizontally polarized Shear wave scattering in an elastic plate," IEEE Trans. Ultrasons. Ferr. Freq. Cont. **34**(4), 461–466 (1987).

[33]Z. A. B. Ahmad and U. Gabbert, "Simulation of Lamb wave reflections at plate edges using the semi-analytical finite element method," Ultrasonics. **52**, 815–820 (2012).
[34]M. V. Predoi, M. Ech Cherif El Kettani, D. Leduc, P. Pareige, and K. Coné, "Use of shear horizontal waves to distinguish adhesive thickness variation from reduction in bonding strength," J. Acoust. Soc. Am. **138**(2), 1206–1213 (2015).
[35]C. Elachi and C. Yeh, "Mode conversion in periodically disturbed thin-film waveguides," J. Appl. Phys. **45**(8), 3494–3499 (1974).
[36]S. R. Seshadri, "Coupling of guided modes in thin films with surface corrugation," J. Appl. Phys. **63**(10), R115–R146 (1988).
[37]B. Le Crom and M. Castaings, "Shear horizontal guided wave modes to infer the shear stiffness," J. Acoust. Soc. Am. **127**, 2220–2230 (2010).